International Scientific Colloquium
Modelling for Electromagnetic Processing
Hannover, October 27-29, 2008

Crucible-free Crystal Growth of Silicon and Germanium – Numerical Simulation and Check by Experiments

M.Wünscher, A. Lüdge and H. Riemann

Abstract

The simulation of Floating Zone(FZ) and Pedestal crystal growth process are presented for both, Si and Ge using the commercial software FEMAG-FZ in axial symmetric approximation. Temperature field, electromagnetic field, and radiative heat exchange (by view factors) were computed under the assumption of a stationary system. The shape of the crystallisation phase boundary was determined by analysing the growth striation of real crystals through the Lateral Photovoltage Scanning(LPS) technique and compared to the simulation. Whereas the crucible-free growth of silicon crystals is common, almost nothing is known about the growth of similar Germanium crystals. The high specific weight and the lower melting point of Ge, in comparison with Si, make the FZ growth very difficult. Some conditions for a stable growth of such crystals were numerically and experimentally investigated.

1 Introduction

We are using the commercial software FEMAG-FZ to simulate the Floating Zone (FZ) and Pedestal crystal growth processes.

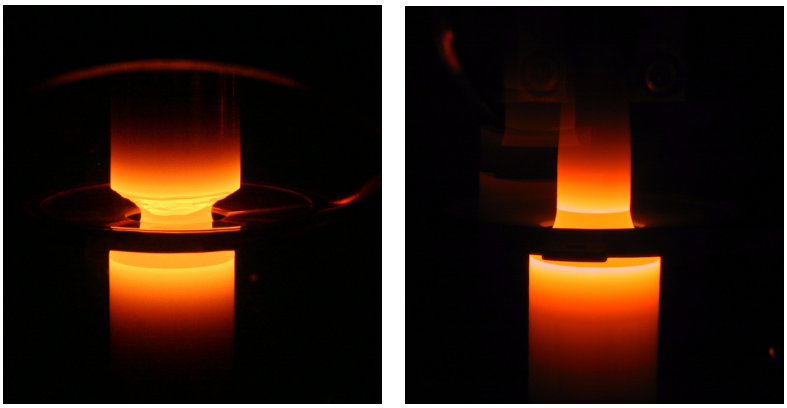

(a) Floating zone ($\varnothing = 40mm$) (b) Pedestal ($\varnothing = 20mm$)

Fig. 1. Two picture of typical crucible free crystal growth processes with silicon.

In Fig. 1a, a picture of a silicon FZ process is shown. Around the darker melt in the middle the induction coil is visible with some reflection on it. Below the melt, the crystal is pulled down and grows with the pulling speed. Above, the commonly polycrystalline feed rod is melted and feeds the melt with liquid silicon. The bevel on the feed rod contains liquid islands which flow into the melt. The surface is called open melt front. The jump of emissivity from the melt to the solid yields to the lightening above and below the melt. The colour change indicate the temperature gradient along the vertical axes. The line between solid and liquid is the trijunction line between melt, solid and surrounding gas in the recipient.

The second picture 1b shows a Pedestal process with silicon. The crystal is pulled out to the top like in a Czochralski process. Contrary to Czochralski the melt is held by the feed rod and not through a crucible. Like in our FZ process, the melt is heated by an induction coil. Because of the opposite direction of the growth you can not apply the needle-eye technique. The maximum diameter is limited by the hole of the coil.

In the next section, the model is described which is used to calculate the position of the phase boundary. This position could be measured after running a crystal growth process using the Lateral Photovoltage Scanning (LPS) technique. Both, experimental and calculated phase boundaries are compared to each other in the last section.

2 Model

Our model is a simplification of the real crystal growth process which take into account the following processes:

- Geometry calculation of the melt surface
- Geometry of the open melt front and the furnace
- Inductive heating of the melt
- Radiative loses along the surfaces
- Temperature field in the system
- Melt convection

Theses processes are modelled in axial symmetric approximation to reduce the amount of calculation power. Also the transient behavior of the process is neglected and the system is solved for stationary case.

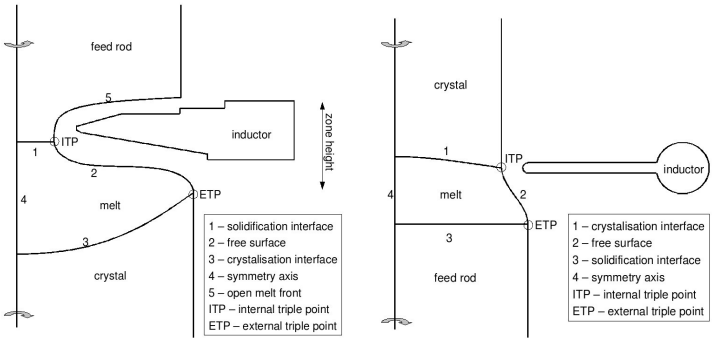

(a) Floating zone (b) Pedestal

Fig. 2. The schematics show the 2D axisymmetric geometrical model of the crystal growth processes.

Fig. 2 shows a typical geometrical model used in the simulation, which is based on the shape of crystal, feed rod, induction coil and recipient. The positions of the triple points are assumed to be known, so you have to define the external (ETP) and internal (ITP) triple points as well as the zone height.

Laplace-Young-Equation

$$P - \rho g z + \frac{1}{2}\rho r^2 \Omega^2 + F_n = \gamma K \tag{1}$$

(P – pressure difference to surrounding gas, r/z – radial/vertical coordinate, Ω – rotation rate, F_n – electromagnetic pressure, K – curvature, γ – surface tension)

For finding the free melt surface, the imposed ITP and ETP are used to solve Eqn. 1. It is clear that you also need to define the two angles in these points to get the unknown pressure P. The angle at the ETP is the growth angle β_0 measured clockwise against the vertical axis. For silicon, $\beta_0 = 11^\circ$ and for germanium, $\beta_0 = 14^\circ$ according to [6, 7]. The angle at the ITP is not so well defined. The experiments show that this point is not stable at one position during the process. One reason is the non-uniform melting of the feed rod. A usefull assumption is setting it to 0°.

FEMAG-FZ uses the finite element formulation to minimise the total energy for solving the Laplace-Young-equation.

The electromagnetic pressure is calculated thought solving the magnetic potential with the boundary element method from Maxwell's equations. This method could be applied, because of the skin effect. For hight frequency the skin depth of the electromagnetic field is given by

$$\delta = \sqrt{\frac{2}{\mu_0 \sigma \omega}} \tag{2}$$

(μ_0 – magnetic permeability, σ – electrical conductivity, ω – rotational frequency)

at which it has decreased by a factor of $\frac{1}{e}$. The current density could be integrated over the interior of the perfect inductor, which yields to a surface current J_S. With the boundary condition along the coil $A_S = \frac{1}{2\pi r} cos\omega t$ and the silicon $A_S = 0$ for the surface potential (dimensionless) this yield to the electromagnetic pressure and the Joulean heating:

$$\underline{q}^{EM} = \frac{\sigma\omega^2\delta}{4}|A_S|^2\underline{n} \qquad F_n = \frac{1}{4}\sigma\omega\left(1+\frac{1}{2}\delta K\right)|A_S|^2 \quad . \tag{3}$$

All other components of the electromagnetic wave are zero[5].

Heat transfer equation

$$c_p \rho \underline{v} \cdot \nabla T = \nabla \cdot (\lambda \nabla T) + \nabla \cdot (\lambda_{add} \nabla T) + \underline{Q} \tag{4}$$

(c_p – heat capacity, ρ – density, T – temperature, T_m – melt temperature,$\underline{r}$ – position vector, λ – heat conductivity, Q – external heat sources)

The heat transfer equation is solved through the finite element method (FEM) on an unstructured grid in the solid(s), the melt(m) and the whole furnace without the gas region. The following boundary conditions are applied:

- open melt front $\lambda(T)\nabla T \cdot \underline{n}|_{OMF} = \underline{q}^{EM} \cdot \underline{n} - \underline{q}_m^{rad} \cdot \underline{n} + h(T - T_m)$
- phase boundaries $(-\lambda_m \nabla T\ |_m + \lambda_s \nabla T\ |_s) \cdot \underline{n}_{ms} = \rho_s \triangle H \underline{n}_{ms} \cdot \underline{v}$
- Continuance along the symmetry axis $\frac{\partial T}{\partial r}|_{r=0} = 0$
- Radiative losses $\underline{q}^{rad} = \underline{\underline{F}} \cdot \underline{T^4}$ modeled through Stefan-Boltzmann-law with view factors $\underline{\underline{F}}$
- electromagnetic surface heat flux $\underline{q}^{EM} = \frac{\sigma\omega^2\delta}{4}|A_S|^2\underline{n}$ for a thin film δ along the crystal, melt and feed rod surfaces
- Water cooled shell $\lambda(T)\nabla T \cdot \underline{n}|_{shell} = 1000\frac{W}{m^2}(T - 300K)$

The positions of the phase boundaries are iteratively searched until a given interface tolerance of 0.001mm is reached and the trijunction point has a tolerance temperature of about 0.001K [4, 3].

The algorithm for the whole coupeled system is shown in Fig. 3b. The local problem takes into account only the melt and the crystal to find the phase boundary between both. If also the melt/feed rod boundary is calculated, then this is also a part of the local problem (Fig. 3a) [1].

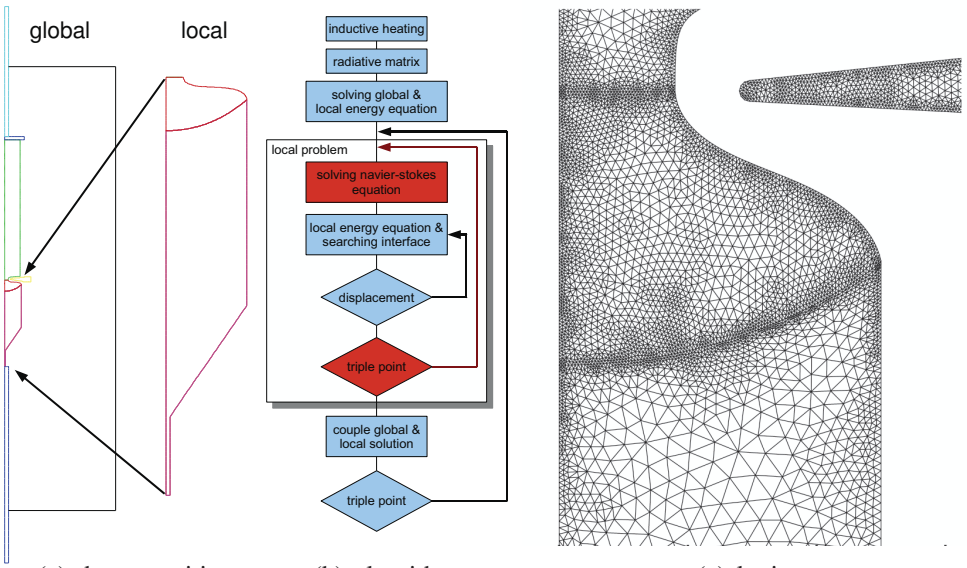

(a) decomposition (b) algorithm (c) lattice

Fig. 3. Splitting the system in a local and global problem (a) to run the algorithm (b) for searching the phase boundaries on the unstructured lattice (c).

The whole system is solved on an unstructured lattice as shown in Fig. 3c. It is adapted to the new boundaries during the iteration. As parameters for the 1D lattice $2000\frac{Points}{m}$ for the phase boundaries of melt and the induction, $400\frac{Points}{m}$ for the feed rod and the crystal as well as $50\frac{Points}{m}$ for all other surfaces are used. From this 1D lattice the 2D lattice is calculated by giving the fraction between the largest and the smallest triangle area A as well as the minimal angle ϕ. Typical values are $(A = 30\ , \phi = 32^{\cdot})$ for the melt, $(A = 200\ , \phi = 30^{\cdot})$ for the solid silicon, $(A = 5000\ , \phi = 30^{\cdot})$ for the recipient and the other parts with $(A = 100\ , \phi = 30^{\cdot})$.

3 Experiment

We made an experiment where the crystal pulling speed was gradually increased. The parameter are given below.

- material: silicon undopted
- feed rod $\varnothing = 65mm$ / crystal $\varnothing = 50mm$
- pull rate: $5 - 8\frac{mm}{min}$
- rotation rate: feed rod 1rpm / crystal 6rpm
- seed: silicon $< 100 >$, edge length 5mm
- gas: argon with 0,15% nitrogen

The pull rate was increased in steps of $0.5\frac{mm}{min}$ and then hold for a while. During this time the floating zone got stable.

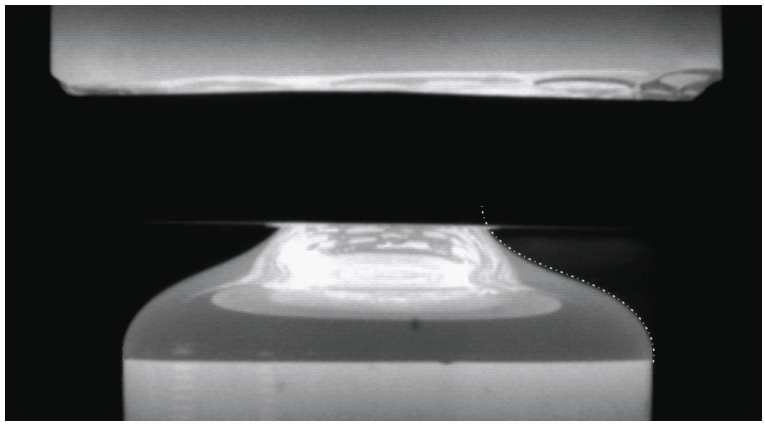

Fig. 4. Picture of the floating zone with the overlayed solution of the Laplace-Young-equation ($v_z = 5\frac{mm}{min}$)

The shape of the free melt surface is recorded by a camera (Fig. 3). To calculate the shape the Laplace-Young-equation is solved and the solution is drawn into the picture. For a defined starting point and starting angle we change the pressure to the surrounding gas until it fits a point near to the induction. In order to find this pressure, we take a Newton algorithm, which will be discused in a later publication. The result is the line in the picture above the melt. Some differences to the real surface are due to the fact that we are neglecting the electromagnetic forces. The ITP position is calculated from the solution at the point where the angle of the curve gets zero to the vertical.

These position are put into the simulation to get the phase boundary between crystal and melt. This boundary is also available through LPS measurements [2], where the striation are visualised.

4 Results

In Fig. 5(a) the simulation of the different pulling rates are shown. The crystal length is chosen like in the experiment. Also, the floating zone is imposed from the fit to the Laplace-Young-equation.

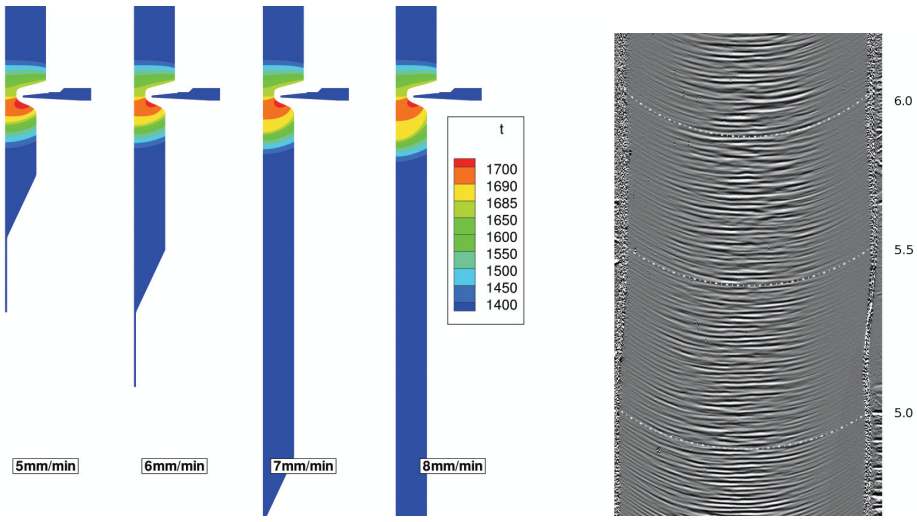

(a) Temperature field (b) LPS measurement

Fig. 5. (a)Calculated temperature field and (b) comparison of the calculated phase boundaries with the LPS picture of the experiment ($v_z = \frac{mm}{min}$).

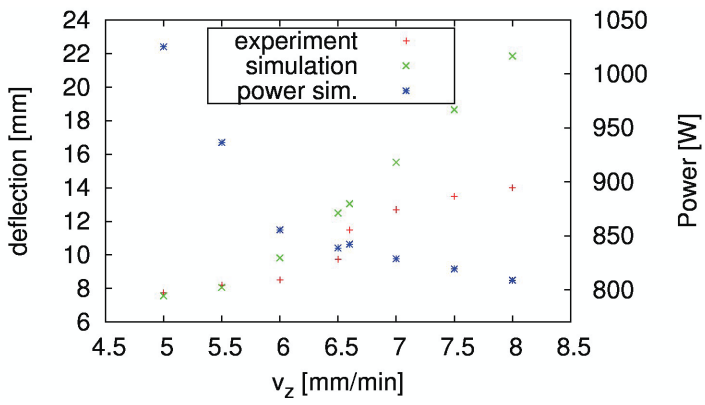

Fig. 6. Deflection and power versus pulling rate

The calculated phase boundary between melt and crystal is drawn into the LPS measurements. The three pulling rates $5\frac{mm}{min}$, $5.5\frac{mm}{min}$ and $6\frac{mm}{min}$ are shown in figure 5(b). The deflection fits very well.

Together with all other pulling rates, a diagram of the deflection versus pulling rate is shown in figure 6. The agreement with the experiment holds not for higher pulling rates. There is no obvious reason, but one can assume that it should

have something to do with the latent heat production and consumption. That is the only parameter where the pulling rate is taken into account. Because of the production at the lower phase boundary the deflection increases. Beside the induced power decreases, because there is no need to induce so much heating at the triple point to get melting point temperature.

Another reason for the hight deflection could be the neglection of the melt motion, which yield to a higher temperature gradient in the melt with a larger deflection of the phase boundary. The test simulation for larger crystals shows that the melt motion reduces the deflection of the phase boundary.

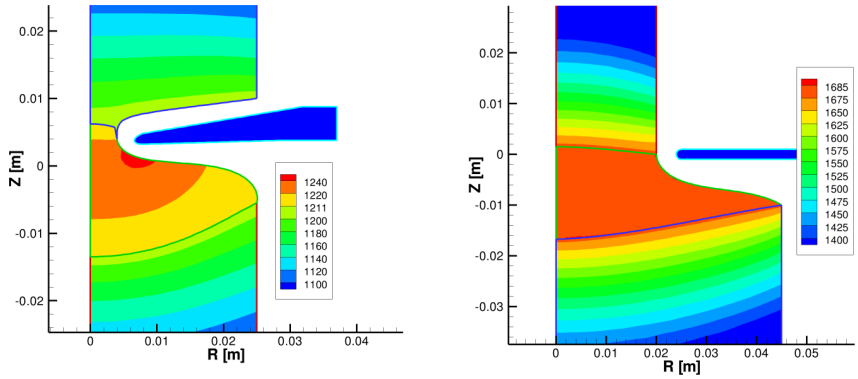

(a) Germanium FZ (b) Pedestal

Fig. 7. Some preliminary results for FZ Germanium (a) and Silicon Pedestal (b)

We have just started to use FZ for germanium crystals. A thinkable configuration is shown in figure 7(a). The main difference to silicon is the higher density which causes a much lower distance between the ITP and the ETP. To get a stable process is a challenge we are working on.

The last figure 7(b) shows a simulation for the Pedestal process. For now we have no input from the experiment to impose the correct position of the triple points. This will be the next step to do as well as the comparison with LPS pictures.

Reference

[1] FEMAG-FZ Guide.

[2] A. Lüdge and H. Riemann. Doping Inhomogeneities in Silicon Crystal detected by the Lateral Photovoltage Scanning (LPS) Method. *Inst.Phys.Conf.Ser. 160*, page 145, 1997.

[3] R. Assaker. Magnetohydrodynamics in crystal growth, 1998.

[4] François Bioul. Use of mathematical expansions to model crystal growth from the melt under the effect of magnetic fields, 1997.

[5] K. H. Lie, J. S. Walker, and D. N. Riahi. Free surface shape and ac electric current distribution for float zone silicon growth with a radio frequency induction coil. *Journal of Crystal Growth*, 100(3):450–458, Mar 1990.

[6] T. Surek and B. Chalmers. The direction of growth of the surface of a crystal in contact with its melt. *Journal of Crystal Growth*, 29(1):1–11, May 1975.

[7] N. Van den Bogaert and F. Dupret. Dynamic global simulation of the czochralski process i. principles of the method. *Journal of Crystal Growth*, 171(1-2):65–76, Jan 1997.

Authors

Michael Wünscher, Dr. Anke Lüdge, Dr. Helge Riemann

Leibniz-Institut for Crystal Growth (IKZ)

Address: Max-Born-Str. 2, 12489 Berlin, Germany

E-Mail: wuenscher@ikz-berlin.de, luedge@ikz-berlin.de, riemann@ikz-berlin.de